Electronic Supplementary Information

A purely ionic voltage effect soft triode

Elalyaa Mohamed[a], Sabine Josten[a] and Frank Marlow [a,b,*]

[a] MPI für Kohlenforschung, Kaiser-Wilhelm-Platz 1, 45470 Mülheim an der Ruhr, Germany
[b] Center for Nanointegration Duisburg-Essen (CENIDE), University of Duisburg-Essen, 47057 Duisburg, Germany
* Corresponding author. Email: marlow@mpi-muelheim.mpg.de

SI-1) Fabrication details[1]

For the top electrode, a metal mesh made of stainless steel (316Ti, Haver & Boecker) with a mesh width of 0.315 mm and a wire diameter d = 0.2 mm was used. The bottom electrodes were wires of same steel material from Edelstahlzieherei Hillesheim GmbH with diameter 0.15 mm. The chemicals used for the coating solutions and for the electrolytes were the same as in our former DSSC works[2,3] and were used as received. Fig. S1 shows the IVEST after a large number of electrical measurements. Its appearance has not changed by the measurements.

Table S1 Special samples. In addition, systematic variations of the X and d parameters have been made (not shown in the table).

Sample type	**Remark**	X_e	X_{TiO2}	d_S / µm	**Sample numbers**
Ib19	basic sample type 2019	1	1	150	156, 156, 169, 174, 177, 180, 217, 237, 242, 271
IoA	optimum sample for amplification	0.6	1	150	274
IoM	optimum sample for a memory	0.16	0.5	1.2	285

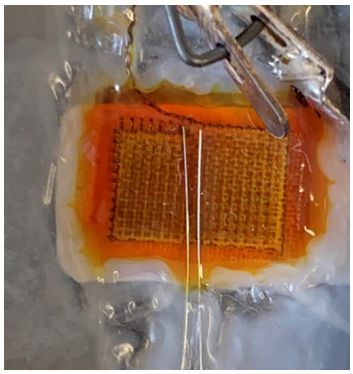

Fig. S1 Optical picture of an IVEST.

SI-2) Measurement configurations

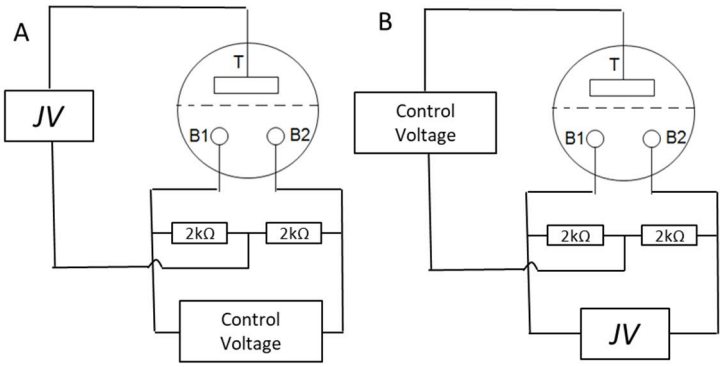

Fig. S2 Schematic description of symmetric BB configuration using JV analyzer. (A) Sym-BB input (B) Sym- BB output

Figure S2A represents the symmetric BB-*JV* configuration to measure the input J_{top}. The bottom electrodes of the IVET are connected to a power supply (DIGI 35 CPU, Voltcraft GmbH) and the top electrode to a home-build *JV* analyzer. Two 2 kΩ resistors were added to assure a symmetric behavior of the bottom electrodes. The current on top electrode (J_{top}) was measured by applying a fixed voltage between the two bottom electrodes (V_{BB}) and using a *JV* analyzer. To characterize the output current (J_{BB}), the top electrode was connected to power supply and the bottom electrodes to the *JV* analyzer as shown in Figure S2B.

SI-3) Device symmetry and reproducibility

a) Device symmetry. For all measurements we have used a sym-BB configuration. To test the symmetry of the device, the same measurements were done with positive and negative V_{BB}. Fig. S3 shows the results for the other read-out direction as in the main text and reveals a good device. The behavior equals the behavior at positive read-out voltages.

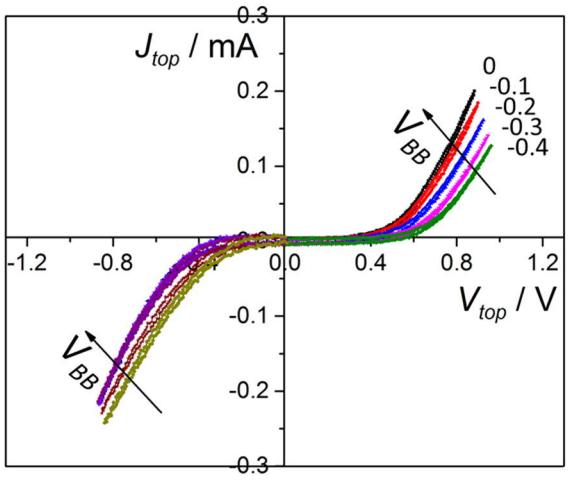

Fig. S3 Symmetric-BB-JV input characterization at negative read-out voltages. The top electrode was connected to the *JV* analyzer. Fixed V_{BB} voltages were applied between -0.4 V and 0 V as indicated by the curve labels (investigated IVEST: 156).

b) Reproducibility. All the measurements were repeated several times with different samples. All samples with same fabrication conditions have shown qualitatively the same behavior at all characterization methods. There was a clear nonlinear dependence of the input current from the input voltage V_{top} and a week dependence of the input current from V_{BB}. For the output measurements, all the samples have shown an increase in R_{BB} by increasing V_{top} as shown in Fig. S3.

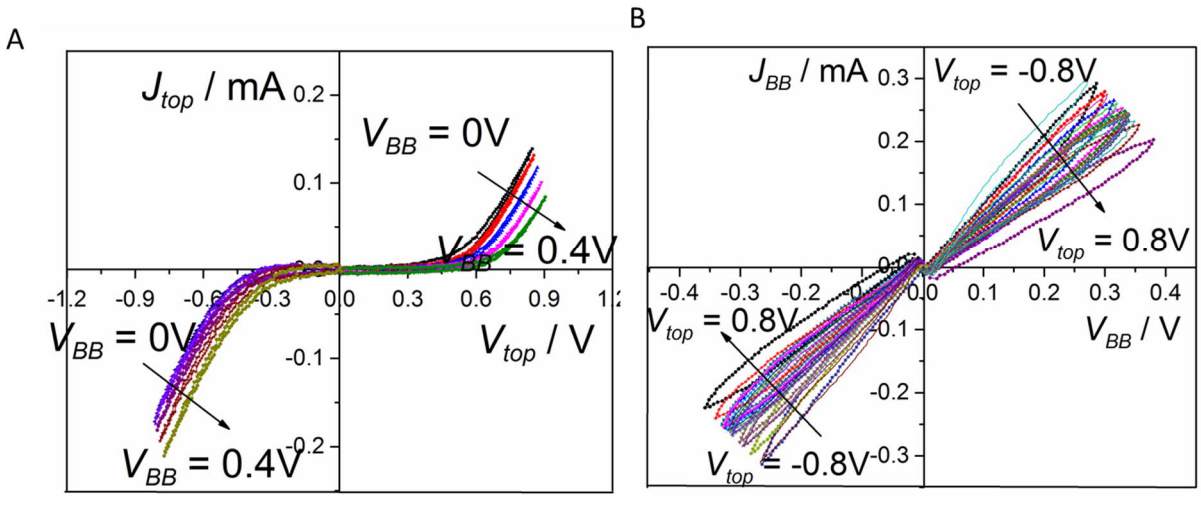

Fig. S4 Another example of an IVEST device (Sample 177). (A) Sym-BB input characteristics. The top electrode was connected to the *JV* analyzer and fixed V_{BB} values were applied from 0 V to 0.4 V. (B) Sym-BB output characteristics. V_{BB} was scanned by the *JV* device while fixed values of V_{top} were applied from -0.8 V to 0.8 V.

The following table shows different samples with same fabrication conditions (where $X_e = 1$, $X_{TiO2} = 1$) at WP1. Fabrication fluctuations induce some differences in the resistance (± 20%) and in the transfer parameter (± 20%).

Table S2 Comparison of different samples

Sample	R_{BB} / kΩ	G_{BB} / mS	g_{BB} / mS/V
156	1.17	0.85	0.43
169	0.87	1.15	0.32
174	1.35	0.74	0.49
177	1.3	0.77	0.48
180	1.34	0.74	0.49
217	0.87	1.15	0.32
237	0.84	1.19	0.31
242	1.23	0.81	0.45
271	0.82	1.22	0.30

SI-4) Amplification calculation

a) General Formula. Differences of our device to standard transistors are the offset of the output current and the highly nonlinear characteristics. Therefore, the description by a modified parameter seems to be more appropriate than the standard description by amplification. Here, the differential amplification factor

$$\beta_{d,WP} = \frac{\partial J_{out}}{\partial J_{in}} \quad \text{(S1)}$$

is used. It describes the small signal behavior and it equals the normal amplification factor for the transistor having a nearly linear transfer characteristics. From the different amplification factors used for transistors, the factor for the common-emitter configuration is the nearest analogue. Since the IVEST output is nearly ohmic, it is useful to re-write the output current as

$$J_{BB} = \frac{V_{BB}}{R_{BB}} = V_{BB} G_{BB} \quad \text{(S2)}$$

leading to the differential

$$\partial J_{BB} = V_{BB} \gamma_{BB} \, \partial V_{top} \quad \text{(S3)}$$

with the specific differential transconductance

$$\gamma_{BB} = \frac{\partial G_{BB}}{\partial V_{top}} \quad \text{(S4)}$$

This definition is equivalent to the eqn 1 and 2 in the main text. Moreover, using the definition of the differential conductance of the top electrode one finds:

$$\partial J_{top} = G_{d,top} \, \partial V_{top} \quad \text{(S5)}$$

Here, one should underline that this differential conductance is strongly voltage dependent. Combining eq S1, S3 and S4 the final result is obtained:

$$\beta_{d,WP} = \gamma_{BB}(V_{top}) \frac{V_{BB}}{G_{d,top}(V_{top})} \quad \text{(S6)}$$

For explicit calculation, we chose the working point WP1: V_{top}= -0.37 V, V_{BB}= 0.25 V. This working point results in the highest amplification among our data. It is a compromise of maximizing γ_{BB} (big G_{BB} slope) and minimizing $G_{d,top}$.

b) Differential conductance. To determine the differential conductance, the setup in Fig. S4A was used. The J_{top} values one gets from:

$$J_M = U_M / (R_M (U_o - U_M))$$

The resulting curve can be fitted with a parabolic curve as shown in Fig S4B. To determine the differential conductance at the working point WP1 = -0.37 V, the tangent at the averaging curve (black curve in Fig. S4B) was used resulting in 0.0217 mS.

c) Amplification calculation. The specific differential transconductance γ_{BB} can be determined from Fig. S3A. At working point WP1 it results in an amplification of

$$\beta = \gamma_{BB}(V_{top}) \frac{V_{BB}}{G_d(V_{top})}$$

$$\beta_{d,WP1} = (-4.57 \frac{\text{mS}}{\text{V}})(\frac{0.25V}{-0.0217\text{mS}}) = \text{-52.6}$$

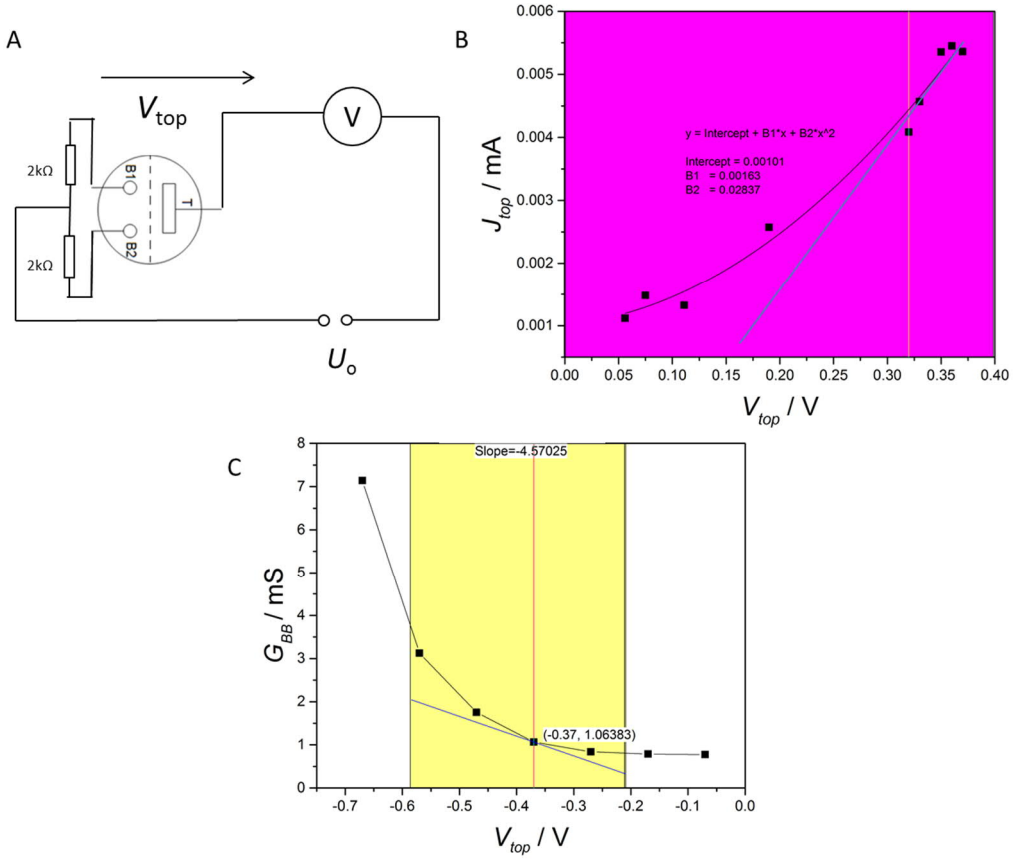

Fig. S5 (A) Set-up used to measure R_{sh}. The inner resistance of the *V*-meter was 10 MOhm. (B) Relation between J_{top} and V_{top}, and a parabolic curve fitted by Origin. The black curve is an average determined by Origin with function Y = intercept+B1X+B2X^2. (C) The dependence of G_{BB} from V_{top} measured for the IVEST device 274. The specific differential transconductance was calculated using the tangent function at WP1 (at $V_{top} = -0{,}37$ V, $V_{BB} = 0.25$ V) with Origin.

SI-5) Stability time calculation

Two meta-stable states are visible in the measurements. They represent the high resistance state (HRS) and low resistance state (LRS). After long times both states are assumed to reach the same resistance R_{BB}^{∞}. It is also assumed that the two states have the same characteristic time τ_2 describing the slow processes. This is considered in the following fitting formulas:

$$L(t) = A_1^L e^{-t/\tau_1^L} + A_2^L e^{-t/\tau_2} + R_{BB}^{\infty} \quad \text{(S8)}$$

$$H(t) = A_1^H e^{-t/\tau_1^H} + A_2^H e^{-t/\tau_2} + R_{BB}^{\infty} \quad \text{(S9)}$$

To avoid the simultaneous fitting of two data sets, the problem is converted to a sequential fitting process for the difference and the sum of the two resistance data. The value for τ_2 is found from fitting the difference with:

$$H(t) - L(t) = A_1^D e^{-t/\tau_1^D} + A_2^D e^{-t/\tau_2} \quad \text{(S10)}$$

The value for R_{BB}^{∞} is found from fitting the sum using the pre-determined value for τ_2:

$$H(t) + L(t) = A_1^S e^{-t/\tau_1^S} + A_2^S e^{-t/\tau_2} + 2R_{BB}^{\infty} \quad \text{(S11)}$$

Eqn S8 and S9 represent the exponential decay at the adaptation and stability time in each state.

Origin2015G was used to analyze the appearing times of the memory states quantitatively as shown in Fig. S4. The fitting of eqn S10 and S11 to the measured data resulted in the adaptation time where $\tau_1 <$ 2 min and in the stability time with $\tau_2 > 2$ min. The time τ_2 resulting from eqn S10 was used as a constant in eqn S11 to calculate R_{BB}^{∞}.

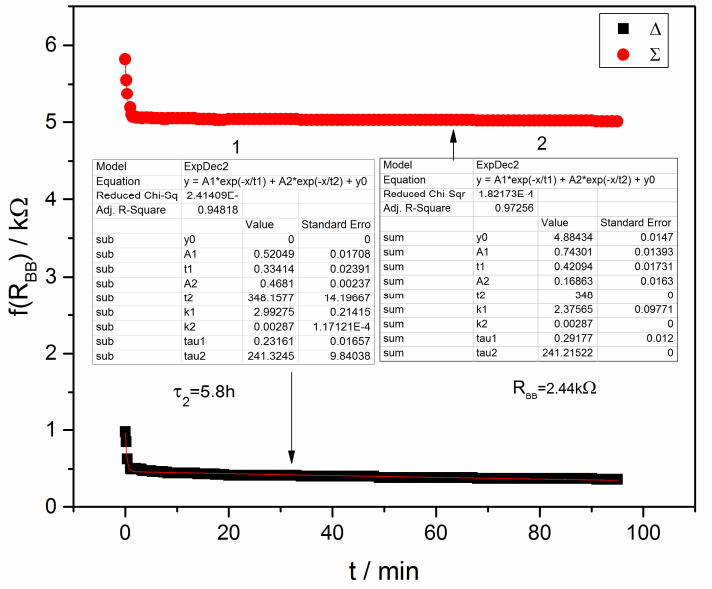

Fig. S6 Analysis of the metastable states. The sum and the difference of the resistance are fitted using Origin2015G. Two characteristic times can be concluded as described in the text. Investigated sample: 285

(v4.3)

[1] F. Marlow, E. Mohamed, S. Josten, German Patent Application, 2022.

[2] F. Marlow, A. Hullermann, L. Messmer, Is the Charge Transport in Dye-Sensitized Solar Cells Really Understood? Advanced Materials 2015, 27, 2447-2452.

[3] S. O. Abdellatif, S. Josten, A. S. G. Khalil, D. Erni, F. Marlow, Transparency and Diffused Light Efficiency of Dye-Sensitized Solar Cells: Tuning and a New Figure of Merit. IEEE Journal of Photovoltaics 2020, 10, 522-530.